Title

Understanding macroscale functionality of metal halide perovskites in terms of nanoscale heterogeneities

Journal

Journal of Physics Energy, 1(1)

ISSN

2515-7655

Authors

Song, Tze-Bin
Sharp, Ian D
Sutter-Fella, Carolin M

Publication Date

2019

DOI

10.1088/2515-7655/aaeee5

Understanding macroscale functionality of metal halide perovskites in terms of nanoscale heterogeneities

Tze-Bin Song[‡], *Ian D. Sharp*[†], *and Carolin M. Sutter-Fella*[‡*]

[‡] Chemical Sciences Division, Lawrence Berkeley National Laboratory, Berkeley, CA 94720, United States

[†] Walter Schottky Institut and Physik Department, Technische Universität München, 85748 Garching, Germany

Corresponding Author

*E-mail: csutterfella@lbl.gov

Keywords

Halide perovskites, nanoscale heterogeneities, structure-function relationship, recombination.

Abstract

Hybrid metal halide perovskites have shown an unprecedented rise as semiconductor building blocks for solar energy conversion and light-emitting applications. Currently, the field moves empirically towards more and more complex chemical compositions, including mixed halide quadruple cation compounds that allow optical properties to be tuned and show promise for better stability. Despite tremendous progress in the field, there is a need for better understanding of mechanisms of efficiency loss and instabilities to facilitate rational optimization of composition. Starting from the device level and then diving into nanoscale properties, we highlight how structural and compositional heterogeneities affect macroscopic optoelectronic characteristics. Furthermore, we provide an overview of some of the advanced spectroscopy and imaging methods that are used to probe disorder and non-uniformities. A unique feature of hybrid halide perovskite compounds is the propensity for these heterogeneities to evolve in space and time under relatively mild illumination and applied electric fields, such as those found within active devices. This introduces an additional challenge for characterization and calls for application of complimentary probes that can aid in correlating the properties of local disorder with macroscopic function, with the ultimate goal of rationally tailoring synthesis towards optimal structures and compositions.

Organic-inorganic metal halide perovskites have attracted tremendous research attention as a fascinating class of semiconductors with applications in low-cost, high performance optoelectronics, including photovoltaics[1,2], light emitting diodes[3], and lasers[4]. In particular, their exceptional photophysical properties, such as high defect tolerance compared to conventional semiconductors[5–8], long diffusion lengths[9], and long lifetimes[10], have motivated studies that attempt to elucidate the physical properties and interactions underlying desirable charge transport mechanisms and dynamics. Although extraordinarily high power conversion efficiencies have been achieved within about 10 years of research, there is a need to better understand mechanisms of efficiency loss and instabilities to facilitate rational optimization of composition. Currently, the field is driven empirically, going from the archetype $CH_3NH_3PbI_3$ to more and more complex chemical compositions, such as $KCsFAMAPbI_{3-x}Br_x$ ($FA = CH(NH_2)_2^+$, $MA = CH_3NH_3^+$), that allow precise tuning of the optical properties, stabilization of desired phases, and mitigation of photoinduced ion migration.[11]

Recent studies have revealed that there can be substantial heterogeneities in polycrystalline metal halide perovskite films.[12–18] These heterogeneities manifest on a variety of different length scales and can significantly influence the underlying structural, transport, and optoelectronic properties. The complex nature of metal halide perovskites has lately evoked the question of "whether their exceptional performance is in fact *as a result of* the length scales and topology of the disorder."[14] While evaluation of operational photovoltaic devices is essential for assessing performance[19], such characterization provides an incomplete picture of internal mechanisms since it samples an ensemble of nanoscale inhomogeneities. Although device characteristics imply that disorder is central to defining function, important questions surrounding the nature of halide segregation, activity of grain boundaries, spatial distribution of defects, and strain remain

unanswered. To address this gap, spectroscopy and imaging techniques can provide important insights into heterogeneities at the nanoscale, with the ultimate promise of unravelling the origin of performance and stability limitations. However, it is crucial to mention that, in contrast to "classical" inorganic semiconductors, there is considerable ionic movement in the perovskites driven by electric fields, illumination, and interface interactions. As a consequence, inhomogeneities can change in space and time, which leads to transient characteristics that are interesting, though generally undesirable for most device applications. Extension of spectroscopies and microscopies to *in situ* characterization of devices or partial device constructs is needed to understand the influence of external drivers.

Complicating mechanistic understandings of heterogeneities in halide perovskites is the correlation of disorder and other material properties to the specific synthesis approach. Perovskite synthesis spans a huge variety of processes including one-step and two-step solution processing, vapor-assisted solution processing, anti-solvent synthesis, and hot casting or vacuum deposition.[20,21] What is clearly missing and could pave the way to a better mechanistic understanding of efficiency loss and instabilities is the rational design of controlled synthesis. This aim will be advanced by use of complimentary nondestructive probes, at times applied *in situ*[22,23] during synthesis, that can correlate the properties of local disorder with macroscopic function; in short, more sophisticated composition/synthesis/function relationships are urgently needed.

With this perspective, we start by considering device level characterization, where the lateral resolution is usually limited to the cell size (typically mm^2 to cm^2). Such measurements are essential to understanding function and identifying bottlenecks to high device efficiency and long-term operational stability. However, the mismatch between the device scale and the natural dimensions defining function, as well as convoluting effects from the absorber itself and interfaces, make

device-level analysis complex and provide an incomplete picture of microscopic mechanisms. Unique features of halide perovskites enable remarkable performance characteristics, but also introduce new complications in how advanced characterization methods are applied. Ultimately, correlating device level characteristics to heterogeneities that arise during synthesis and evolve during operation requires application of complimentary methods. Concerted application of such approaches offers promise to reveal critical roles of heterogeneity for optimization of the perovskite composition and routes to their synthesis. This paper emphasizes the archetypical methylammonium lead halide compound ($MAPb(I_{1-x}Br_x)_3$), which is the most intensively studied composition to date, and highlights the more generally applicable characterization methods that can be applied across compositions. Importantly, experimental methodologies and fundamental insights gained through years of intensive study of this material system serve as a foundation for rapid progress in understanding more recently evolving and more complex compositions. In this respect, a few of the numerous knowledge gaps associated with nanoscale heterogeneities in complex metal halide perovskite compositions are highlighted and compared to the more traditional $MAPb(I_{1-x}Br_x)_3$ system.

Device level characterization

Current density-voltage (J-V) curves are commonly used to characterize the conversion efficiency of solar cells and provide quantitative numbers for the key photovoltaic parameters - open circuit voltage (V_{oc}), short circuit current density (J_{sc}) and fill factor (FF), while external quantum efficiency (EQE) measurements provide information on the spectrally resolved photon conversion efficiency (examples for a planar FTO/TiO_2/$MAPbI_{3-x}Br_x$/Spiro-OMeTAD/Au device structure are shown in Figures 1a, b).[24] In perovskite devices, serious hysteresis in J-V characteristics has been observed, resulting in significant differences in apparent device

efficiencies depending on the voltage scan direction and scan rate.[25-28] Proposed mechanisms include dynamics of defect states[29,30] and related ionic movement.[31–33] It is generally suspected that the hysteresis arises from fundamental properties of the perovskite material but its manifestation is strongly dependent on its interfaces and interaction with other layers.[36,37] Due to this hysteresis effect, researchers commonly use the steady state maximum power output or hysteresis factors to provide better evaluation of the device performance, rather than the traditional method of simply using J-V curves.[38–41]

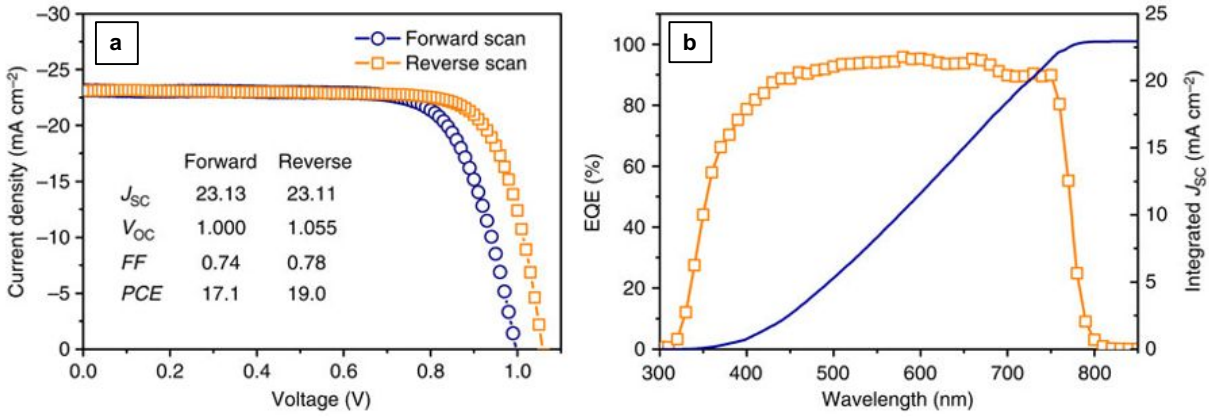

Figure 1 Device Level Characterizations. a) Current density-voltage (J-V) curves in forward and reverse scan direction of a FTO/TiO_2/$MAPbI_{3-x}Br_x$/Spiro-OMeTAD/Au device. b) Corresponding external quantum efficiency (EQE) spectrum and integrated current density curve. Reprinted with permission from Reference [24]. 2016 Nature Publishing Group Copyright.

Several reports have demonstrated significant reduction or elimination of the hysteresis effect by various strategies. For example, a universal KI doping approach was demonstrated to be successful for $FAMAPbI_{2.55}Br_{0.45}$, $FAMACsPbI_{2.7}Br_{0.3}$, $MAPbI_3$, and $FAPbI_3$ perovskites and was explained by reduced bulk trap density and low-frequency capacitance.[42] Similarly, impurity phase management via incorporation of RbI was shown to improve charge carrier mobility and lifetime,

as well as to suppress hysteresis in RbMAFA halide perovskites.[43] A different approach, namely realization of nearly ideal energy level alignment of the hole transport layer, eliminated hysteresis in $MAPbI_3$ solar cells completely and was reasoned to be related to diminished interfacial charge accumulation.[36] Also, the passivation of surface trap states and/or states along grain boundaries via fullerene deposition represents a promising route to fabricate hysteresis-free $MAPbI_3$ devices.[37] These findings point towards ion motion being a key contributing factor. In the absence of grain boundaries, ion motion is mediated by vacancies. To which extent the organic cation is mobile is currently under investigation. It is crucial to consider that these device level characteristics are determined using structures on the mm^2 to cm^2 scale. They reveal, however, properties of driven point defect heterogeneities down to the nm scale. While such processes are implied by these measurements, understanding the underlying mechanisms requires more advanced characterization.

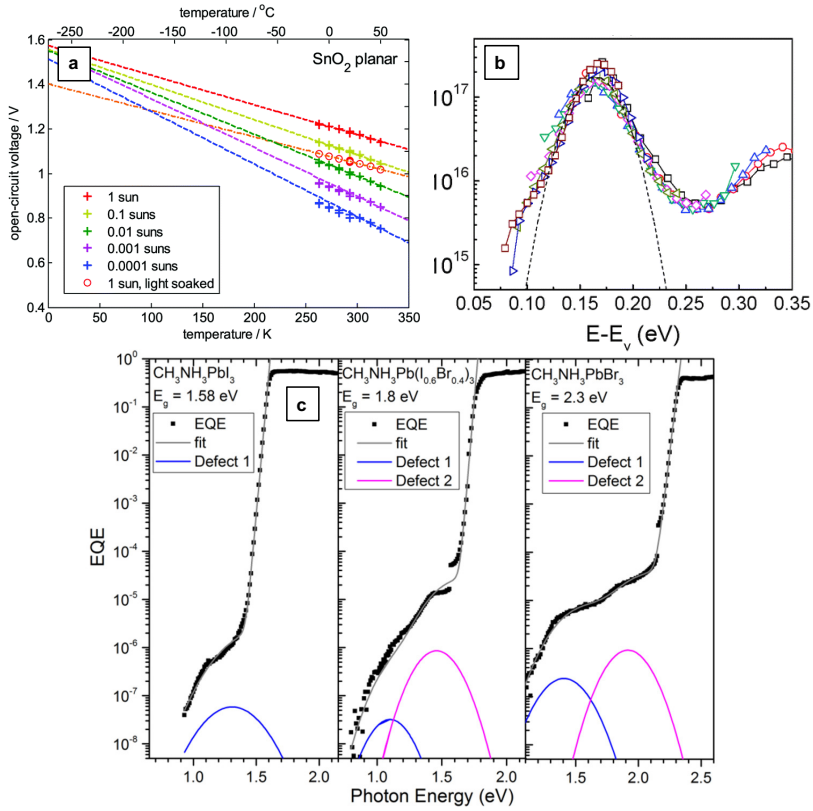

Figure 2 Device Level Characterizations. a) Temperature dependent V_{oc} of a FTO/SnO_2/CsMAFAPb($I_{0.83}Br_{0.17}$)$_3$/ Spiro-OMeTAD/Au device at different light intensities. b) Defect energy distribution of a perovskite device after energy conversion from capacitance-voltage (C-V) measurements at different temperatures. c) Sub-bandgap EQE spectra for $MAPbI_{3-x}Br_x$ perovskite devices with x = 0, 0.4, and 1. Fits to the data are shown as solid gray lines, with the underlying Gaussian defect distributions shown as solid blue and magenta lines. a), b), and c) reprinted with permission from References [19, 44, 45]. 2017 Royal Society of Chemistry (a), 2015 Royal Society of Chemistry (b), and 2017 American Chemical Society (c).

Deeper device analysis to illuminate performance limitations include temperature-dependent and light-intensity-dependent J-V,[19,46,47] admittance spectroscopy (AS),[44,48–50] and sub-bandgap external quantum efficiency (EQE).[29,45] These approaches are widely used in semiconductor research and will be briefly discussed next.

Temperature-dependent and light-intensity-dependent J-V characterizations not only provide device efficiency trends under various operational conditions but also insights into loss mechanisms.[51] Temperature-dependent hysteresis effects suggest that multiple charging-discharging processes are responsible for the previously described hysteresis.[52] Tress *et al*. reported on a comprehensive study using temperature-dependent and light-intensity-dependent J-V characterization on state-of-art mixed ion ($CsMAFAPb(I_{0.83}Br_{0.17})_3$) perovskite devices (Figure 2a) to distinguish the dominant recombination loss mechanisms using different device architectures. In brief, it was found that optimized devices with V_{oc} ~1.2 V exhibit ideality factors (n_{ID}) ~1.6 and $E_a = E_g$ (with E_a being the activation energy of recombination and E_g the bandgap energy, respectively) which indicates recombination is dominant in the bulk absorber.[19] This conclusion is surprising due to findings discussed below (section: **Nanoscale absorber level characterization**) where significant numbers of surface defects with inhomogeneous lateral distribution have been observed by photoluminescence spectroscopy and shown to be healed by surface passivation. Thus, it is speculated that devices characterized by Tress *et al*. might have had nearly ideal contact formation.

AS measurements provide another piece of the puzzle by investigating the concentration of defects and their energetic positions. These defect properties can be correlated with their device parameters and used to guide processes and materials towards high performance devices. The AS measurement utilizes the capacitance responses from the charging and discharging of defect states by modulating the bias voltage to extract the spatial charge distribution. This measurement yields the activation energy of the major defect state (E_d) and the defect distribution density within the bandgap, as illustrated in Figure 2b (measured at different temperatures). The major defect states observed in $FTO/TiO_2/MAPbI_3/Spiro\text{-}OMeTAD/Au$ devices include a major shallow-defect peak at 0.167 eV and a deep-level defect higher than 0.3 eV above the valence band.[44] The integrated

densities of the major defect states in both cases are ~10^{16} cm^{-3}, which lie within the broad range of later reports, where values of ~10^{15} to 10^{17} cm^{-3} were found.[48,49,53,54] AS measurements sample an ensemble and are limited by assumptions about system homogeneity that can mask nanoscale heterogeneity. More specifically, the defect positions relative to the band edges are based on the assumption of the majority charge carrier type of the material, whereas doping in perovskites is poorly controlled.

The presence of defects has also been found by sub-bandgap EQE measurements (Figure 2c).[45] The response in sub-bandgap EQE measurements corresponds to transitions from bound to free electronic states that generate the photocurrent. Similar to AS, the sub-bandgap EQE measurement does not directly indicate whether the observed transitions are caused by trapped holes or electrons that are excited to the valence or conduction band, respectively. The energetic position of the sub-bandgap defect spectrum in FTO/TiO_2/$MAPbI_3$/Spiro-OMeTAD/Au devices was observed around ~ 1.36 eV, which is ~ 0.2 eV away from the band edge and consistent with the results from AS measurements.[45] Sub-bandgap EQE on mixed I/(I+Br) perovskites revealed the presence of a second defect extending into the bandgap that could explain the observed voltage losses in pure Br $MAPbBr_3$ devices.[45] This finding suggests the presence of deep defects in mixed I/(I+Br) perovskites and ties back to low photoluminescence quantum yields in $MAPbBr_3$ as discussed later. Other defect states have been reported for FTO/TiO_2/$MAPbI_3$/Spiro-OMeTAD/Au with a deep-level defect state at 0.76 eV by Miller *et al.*, which might be related to specific device preparation conditions and device quality.[29] By combining sub-bandgap EQE measurements with transient photocapacitance spectroscopy (TPC) they found that such a deep-level defect may be present at the interface or originates from outside the perovskite layer.[29] In general, there appear to be frequent discrepancies in the detection and assignment of defect levels in halide perovskite materials that

possess nominally identical composition. This gap likely points towards the importance of synthesis conditions in defining defect concentrations and distributions, but a systematic investigation does not yet exist.

It is important to note that there is clear evidence for a reduction in bulk and surface defect density when combining multiple cations in halide perovskites with decreasing defect density from MAFA > CsMAFA > RbCsMAFA.[55] An outstandingly high V_{oc} of 1.24 V in a quadruple cation perovskite device (FTO/compact-TiO_2/mesoporous-TiO_2/RbCsMAFAPb$(I_{1-x}Br_x)_3$/Spiro-OMeTAD/Au) with E_g = 1.63 eV was attributed to a major suppression of non-radiative recombination sources and reduced defect density.[55] Cation engineering was recently reported to heal deep defects in wide bandgap CsMAFAPb$I_{3-x}Br_x$ (x = 0.25 and 0.4) compounds.[56] Using density functional theory (DFT) calculations this was attributed to the presence and reorientation of the dipolar MA cation which led to the absence of a second, deeper trap level.[56] Interestingly, this work stated that incorporation of MA might not reduce the formation of defects but rather leads to a passivation of deep defects. It is possible that such self-healing mechanisms are related to findings by theorists pointing out that perovskites are electrically benign and highly defect tolerant.[5,57] As new compositions are explored, additional internal self-passivation processes may be discovered and it will be important to examine mechanisms by which they occur, especially with respect to mixed cation systems, in order to rationally optimize materials.

Macroscale absorber level characterization

Following the principle of detailed balance, if one considers a solar cell device at open circuit, where no current is flowing, all photons with $h\nu > E_g$ are absorbed and create electron-hole pairs whose lifetimes are finite, i.e. they must ultimately recombine. In order to reach the Shockley-

Queisser (SQ) limit the only recombination mechanism should be radiative.[58] In this regard, photoluminescence quantum yield (PLQY) measurements are a powerful method to assess the relationship between radiative and nonradiative recombination. The dependence of the external (measured) PLQY on the illumination density for mixed halide $MAPbI_{3-x}Br_x$ perovskites is shown in Figure 3a.[59] Given the fact that ionic movement in the perovskite can result in inhomogeneities that change in space and time under non-equilibrium conditions, it is important to note that these PLQY measurements were performed without light soaking and before the appearance of any halide segregation (that is illumination induced demixing of I-Br compositions to form I-rich and Br-rich domains). The external PLQY first increases with increasing pump-power density, before it then reaches a plateau and eventually decreases at the highest pump-power densities used in this study due to dominant Auger recombination. The rise in PLQY at low excitation intensity has been observed by multiple groups for metal halide perovskites[59–62] and has been explained, in conventional manner, by gradual filling of trap states at low excitation until radiative recombination dominates when the trap states are filled.[60,62] $MAPbBr_3$ shows a significantly lower PLQY compared with $MAPbI_3$ or mixed I/(I+Br) compositions. This finding can be related to the sub-bandgap EQE findings, where deep level defects were observed for pure $MAPbBr_3$.[45] Although perovskites are predicted to be defect tolerant, the PLQY measurements reveal considerable losses and illustrate that metal halide perovskites are limited by nonradiative SRH recombination at low excitation intensity, including 1-sun.[59,62,63]

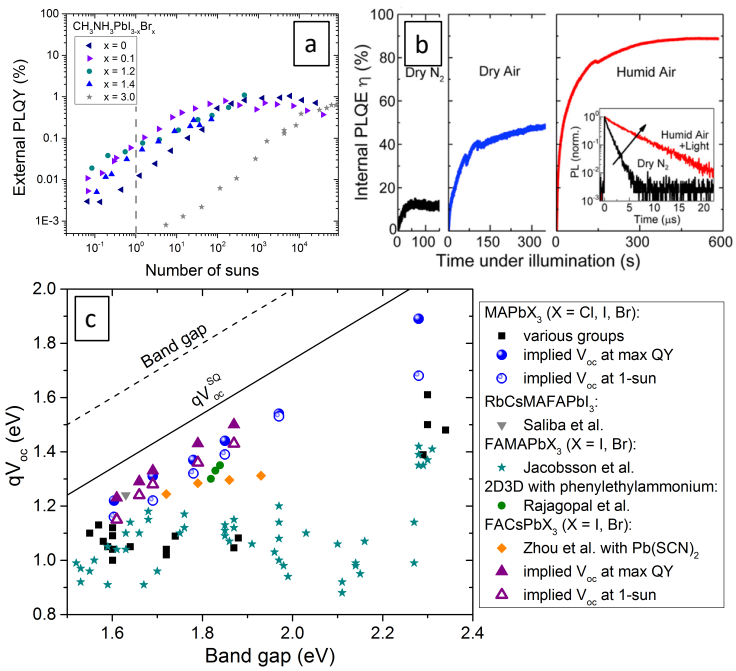

Figure 3. Macroscale Absorber Level Characterizations. a) External photoluminescence quantum yield of $MAPbI_{3-x}Br_x$ films as a function of injected carrier density. b) Internal PLQY of $MAPbI_3$ films recorded over time under constant illumination in dry N_2, dry air, and humid air. c) Optically implied V_{oc} in comparison to electrically reported V_{oc} of various metal halide perovskite compositions: $MA = CH_3NH_3^+$, $FA = CH(NH_2)_2^+$. a) Adapted with data previously published in Ref.[62]. b) Reprinted with permission from Ref.[64]. Copyright 2017 Elsevier Inc. c) prepared from data published in References [49, 58, 60, 62–64]

It is crucial to recognize that unique properties of metal halide perovskites, such as light-induced ion migration and halide segregation, surface reactivity with the environment, and the co-presence of PbI_2 phase, can significantly affect PL emission intensities. As an example, the atmospheric condition under which the PLQY is recorded plays a critical role.[64,69] Brenes *et al.*, showed a substantial improvement in humid air versus dry N_2 or dry air, reaching internal PLQY values close to 90%.[64] Here, the internal PLQY is calculated from the measured external PLQY following the approach introduced by Richter *et al.*[70] Correspondingly, the minority carrier lifetime significantly increased, as depicted in the inset of Figure 3b.[64] To explain the improvements in humid air, it has

been proposed that the photo-induced reduction of O_2 to O_2^- shifts shallow defect levels into the valance band, thus eliminating shallow defect levels.[64] These observations tie back to the role of the synthesis atmosphere, the reaction of the material with atmosphere, and how it could be employed to tailor better device performance and stability.

As a consequence of optical reciprocity, quantitative photoluminescence can serve as an invaluable measurement to derive one of the key parameters of a solar cell device, the open-circuit voltage (V_{oc}):[71–74] $qV_{oc} = \Delta E_F \approx kT \ln\left(\frac{J_{sc}}{J_0}\right) + kT \ln PLQY_{ext}$, where q is the elementary charge, ΔE_F the splitting of the quasi Fermi energies, and $kT \ln\left(\frac{J_{sc}}{J_0}\right) = V_{oc}^{SQ}$, with V_{oc}^{SQ} being the V_{oc} in the SQ limit in which only interband radiative recombination occurs[58], J_{sc} the short circuit current density, and J_0 the saturation current density. As mentioned above, any nonradiative recombination loss will lead to a voltage drop, and thus a loss of efficiency in a PV device. In the ideal case, the external PLQY (which is a number ≤ 1) is 1 and thus $qV_{oc} = qV_{oc}^{SQ}$.

The optically extracted (implied) V_{oc} serves as an upper limit for the maximum achievable V_{oc} purely based on the intrinsic material properties in the absence of effects associated with non-ideal selective contacts or subsequent processing steps that could lead to enhanced nonradiative recombination losses. Figure 3c summarizes the implied V_{oc} values for $MAPbI_{3-x}Br_x$ and $FACsPbI_{3-x}Br_x$ perovskites calculated for the highest external PLQY measured, as well as for the PLQY at 1-sun (i.e., the PLQY obtained from intensity-dependent PLQY measurements[59,65]). These are compared to the electrical V_{oc} values reported for solar cell devices as a function of the absorber bandgap for different perovskite compositions including multi-cation and mixed 2D-3D perovskites. The clear discrepancy between implied and electrically measured V_{oc} illustrates nonradiative losses at the contacts and was also pointed out in Ref.[63]. Together with PL

measurements discussed before, as well as the device analysis by Tress *et al*., it appears that there are important losses in both the absorber itself and at its interfaces. It is known that wider bandgap mixed I/(I+Br) compositions (particularly MA-perovskites) show photo-induced halide demixing, which limits the device V_{oc} as can be seen in Figure 3c between ~ 1.7 eV < E_g < 2.2 eV.[75] Interestingly, this halide demixing is significantly mitigated in mixed cation perovskites.[11,65,76] Mechanisms proposed to reduce this photo-induced effect include mixed halide phase stabilization via build-up of strain[65] and removal of halide vacancies in combination with immobilization of excess halides via electrically benign potassium-halide species that accumulate at grain boundaries and surfaces[11]. The exact mechanisms are still under investigation, with leading hypotheses based on strain affecting thermodynamics or vacancy concentrations primarily impacting kinetics. These are fundamentally different, though not necessarily mutually exclusive, mechanisms that involve complex interactions at the nanoscale. Improved understanding of the underlying processes will be important for designing stable absorbers with engineered bandgaps, which will be aided by probing these processes at their natural scales, as discussed below.

Another way to increase the bandgap is by interrupting the 3D perovskite structure by insertion of bulky cations, which form 2D structures (e.g. phenylethylammonium). These mixed 2D-3D perovskites clearly outperform their 3D counterparts with equivalent bandgaps and reach high device V_{oc} values (green circles in Figure 3c).[66] One hypothesis is that interruption of the 3D crystal by 2D layers provides a way to limit ionic movement and, thus, induced heterogeneity. On the other hand, hysteresis is observed in both 3D and 2D perovskite solar cells, indicating that the underlying mechanisms causing hysteresis exist in both, even though ionic transport should be significantly limited in vertically aligned 2D perovskite devices.[77] 2D-3D perovskites are also used as passivating layers, e.g. on bulk $FAMAPbI_{2.55}Br_{0.45}$ films, and have been found to enhance stability

as well as power conversion efficiency.[78] The proposed mechanisms are deactivation of surface traps and reduction of ionic movement via an interfacial energetic barrier.[78] Given these beneficial effects we anticipate more and more research with focus in this direction.

Overall, quantitative photoluminescence measurements provide a bridge between material properties of the absorber and the characteristics of devices. In particular, they reveal limitations of the absorber due to nonradiative recombination via defects, especially at low illumination densities, and recombination at selective contact interfaces. Similarly, PL can detect photo-induced halide demixing in mixed I/(I+Br) perovskites, which is reflected in changing spectral emission due to formation of I- and Br-rich domains under illumination. Such halide segregation leads to a much lower V_{oc} relative to the bandgap of the mixed I/(I+Br) compounds. Thus, PL is a powerful method for connecting different length scales.

To this point, we have not addressed electronic transport properties (such as minority carrier lifetime τ, diffusion length L, and mobility μ linked via $L = \sqrt{kT \cdot \mu\tau/q}$, with the Boltzmann constant k, the absolute temperature T, and the elementary charge q) that determine function (e.g. V_{oc} and J_{sc}). Considerable research has been devoted to understanding these critical parameters using a wide range of different methods. For example, mobilities have been determined by transient and steady-state methods such as Time of Flight (ToF), Time-Resolved Microwave Conductivity (TRMC), Hall effect measurements, or THz spectroscopy.[79] Reported values vary by about 2-3 orders of magnitude (e.g. < 1 – 70 $cm^2/(Vs)$ reported for $MAPbI_3$).[79,80] However, it is worth mentioning that the different techniques sample "different mobilities" because of the different length scales that are probed – from the very local all-optical methods to the macroscopic long-range electrical methods – and "different carriers" under illumination or in darkness. By comparing

values obtained from methods that naturally probe interactions over very different length scales (i.e. THz vs. ToF), it is possible to gain improved insight on how different factors, such as electronic structure, electron-phonon interactions, grain boundaries, and interfaces, impact charge transport, even if the methods themselves are not spatially resolved.[79]

Nanoscale absorber level characterization

Exploiting the capabilities of advanced characterization techniques to resolve structural, optical and electrical properties at the nanoscale, it becomes evident that there are substantial heterogeneities in polycrystalline metal halide perovskite thin films that determine macroscale device performance metrics, transient characteristics, and synthetic reproducibility. In recent years, imaging or mapping techniques, including PL imaging[14,15,64,81,82], cathodoluminescence (CL) imaging[16,83], atomic force microscopy (AFM)[17,84], scanning micro X-ray diffraction (XRD)[14], electron beam-induced current (EBIC)[85], scanning near-field optical microscopy (SNOM)[82], Kelvin probe force microscopy (KPFM)[86–88], transmission electron microscopy (TEM)[14,89], as well as non-laterally resolved techniques based on X-ray absorption spectroscopy[90–92], X-ray photoelectron spectroscopy[93], and solid-state nuclear magnetic resonance (NMR) spectroscopy[94–96] have been adopted to characterize local properties of metal halide perovskites.

Broad spatial distributions of PL intensity, significant grain-to-grain heterogeneities, and spectral emission shifts have been reported for polycrystalline perovskite films. Draguta *et al*. pointed out extreme spatial heterogeneities in recombination dynamics of $MAPbI_3$ with some regions dominated by bimolecular radiative recombination while others show the signature of carrier trapping.[15] As a consequence, the PLQY also shows lateral variations (compare Figure 4a).[15] Ultimately, those spatially heterogeneous properties were found to extend over length scales larger

than the crystalline domain sizes.[15] This is interesting because it raises the question of whether grain to grain variations or, rather, longer range heterogeneities that are decoupled from the grain structure are dominant in defining lateral variations in loss processes. In a different study on nonstoichiometric $MAPbI_3(Cl)$ a PL intensity drop of ~65% has been observed at grain boundaries[18] (Figure 4b). Additionally, Cl-rich regions in $MAPbI_3(Cl)$ were correlated with higher PL signal and a vapor pyridine treatment was found to heal weakly luminescent domains.[81] Recently, Braly *et al*., demonstrated a PLQY of > 90% after n-trioctylphosphine oxide (TOPO) surface treatment of $MAPbI_3$.[97] TOPO acts as an electron donating molecule binding to the $MAPbI_3$ surface and thereby reduces nonradiative recombination[97], an effect that has been observed with other Lewis bases as well[10]. Not surprisingly, the surfaces of metal halide perovskite films are critical to performance. Both, chemical surface treatment of the light absorber and addition of passivation layers to selective contacts lead to reduced interface defect concentrations and are getting more and more research attention. The fact that surface treatments make dark grains bright as measured by PL implies an inhomogeneous lateral distribution of surface states. The respective trap-state densities for bright versus dark PL regions vary starkly, from $< 1\times10^{15}$ cm^{-3} to 9×10^{17} cm^{-3}, respectively (Figure 4a).[14,15,18] A huge spread of defect densities for similar material compositions calls, in our opinion, for the need of better understanding of the influence of the synthesis parameters on local material properties and surface passivation. In this respect, not just ex situ nanoscale probes, but in situ spectroscopies and microscopies during synthesis and processing, have great potential to enhance understanding of synthesis-property relationships.

High resolution CL microscopy, in which electron beam-induced luminescence is detected along with secondary electrons as a function of excitation position, provides detailed insights into spatial distributions of the luminescence yield correlated to morphology.[16] CL microscopy confirms high

variability in luminescence and hence radiative versus nonradiative recombination rates from grain to grain.[16] Additionally, depth dependent information can be inferred by tuning the electron acceleration voltage to reveal distributions in surface and bulk trap density.[16] Figure 4c illustrates CL images of $MAPbI_3$ films on FTO/TiO_2 taken at accelerating voltages of 1.5 kV (left) and 5 kV (right). The corresponding depths where 75% of the energy is deposited are 25 and 100 nm, respectively. The highest CL fluctuation between grains has been observed at the film surface (i.e. high intensity contrast) which indicates very heterogeneous surface trap densities while the defect distribution in the bulk appears more homogeneous (Figure 4c).[16] This observation is consistent with findings from laterally resolved PL measurements on perovskite films without chemical surface passivation treatment (discussed above). A consideration to keep in mind here is that hybrid perovskites are soft materials which degrade under various circumstances and "*harsh*" measurement conditions. High e-beam energy can alter the perovskite properties by causing defect formation and phase transformation.[98] It was found that the degree of damage not only depends on the cation ($CsPbI_3$ is more resistant than $MAPbI_3$ or $FAPbI_3$) but also on the defect density of the perovskite material.[98] In addition, it was found that the electron beam can induce ion redistribution in $MAPbI_3$.[99] This means CL is a powerful technique but extreme care must be taken in avoiding beam damage and, thus, evolution of artifacts caused by the energy of the probe.

Not only spatially resolved luminescence-based measurements point towards variation in trap densities (laterally and spatially), a recent diffraction study by Jones *et al*. for the first time revealed how the variation in trap states ties to local strain distributions associated with halide vacancies.[14] In this study, crystallinity investigated via scanning micro X-ray diffraction revealed strain-related defects and the existence of local grain clusters.[14] Figure 4d depicts the local map of the peak scattering vector q of the $\langle 220 \rangle$ diffraction peak (left) and selected slices (paths d+e) through the

map (right). Using a first principles atomic model it was shown that introduction of compressive strain (using the relative shift of the q value) increases the concentration of charged iodide vacancies by a factor of 2 compared to the unstrained crystal.[14] It appears that the soft nature of the perovskite lattice is prone to local lattice contraction caused by a defect.[14] Distinct local patterns were found as evidence for regions with similar crystallographic properties called super-grains due to their dimensions being more than 10× larger than individual grains.[14] This is even more extreme in triple cation MAFACsPbI$_{3-x}$Br$_x$ perovskites with super-grains being more than 1000× larger than single grains.[14] Jones *et al*. suggest, that the super-grain size is the critical size that can be correlated to device performance and not the grain size extracted from SEM images.[14] In agreement and confirmed with PL mapping, spatially heterogeneous properties were found to extend over length scales larger than the crystalline domain sizes.[15] These findings not only link optical and structural properties on different length scales but also raise questions of, what is the origin of super-grains and how do they influence the overall device performance, is it grain to grain variation or, rather, longer range heterogeneities that are decoupled from the grain structure that define lateral variations in loss processes?

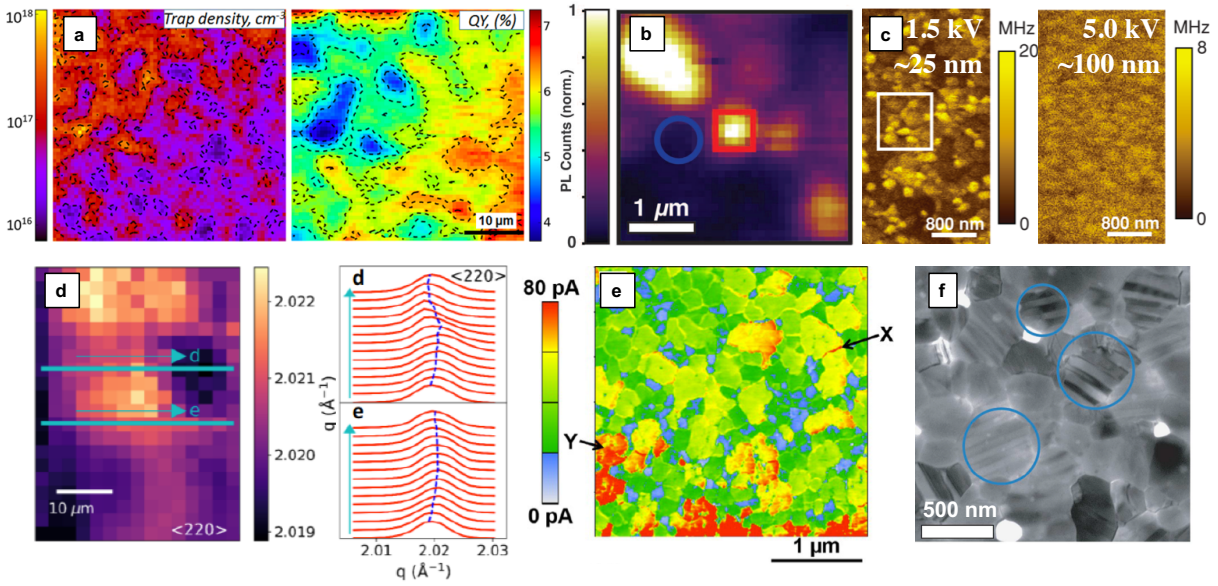

Figure 4. Nanoscale Absorber Level Characterizations. a) Trap density map (left) and corresponding external PLQY (right). b) Confocal PL image highlighting a bright (red square) and dark region (blue circle). c) CL images taken at accelerating voltages of 1.5 (left) and 5.0 kV (right) and the corresponding depth within which 75% of the energy is deposited. Please note the different intensity scales. d) ⟨220⟩ diffraction peak *q* map with lines indicating paths d and e (left) and traces of the ⟨220⟩ diffraction peak taken along paths d and e (right). e) Two-dimensional photocurrent map. Positions "x" and "y" are discussed in the text. f) Room temperature bright-field TEM image of a $MAPbI_3$ film. Blue circles depict stripe contrast in some of the grains. a), b), c), d), e), f) reprinted with permission from References [15, 18, 16, 14, 17, 89]. 2016 American Chemical Society (a), Copyright 2015 American Association for the Advancement of Science (b), 2015 American Chemical Society (c), permission received from the authors (d), 2016 American Chemical Society (e), 2017 Nature Publishing Group (f).

Photoconductive AFM on partial solar cell device stacks (e.g. FTO/TiO_2/perovskite) is a powerful technique to directly link grain-to-grain and intra grain heterogeneities to device metrics, such as short-circuit current (I_{sc}), V_{oc}, and *FF*.[17,84] For example, Kutes *et al*. mapped the local photovoltaic performance parameters of solution processed $MAPbI_3$-based half devices with nanoscale resolution.[17] This work illustrated interconnected aggregates of super-grain structures exhibiting similar magnitude of I_{sc} and heterogeneous transport between interconnected grains and

grain boundaries (Figure 4e).[17] The "x" marker in Figure 4e illustrates a grain boundary with enhanced I_{sc} while the "y" marker depicts a region (yellow) with lower I_{sc} within an area of similar topography (red). Thus, topography-related artifacts are negligible in this case.[17] In a different study on $MAPbI_{3-x}Cl_x$ (synthesized via a two-step vapor-assisted solution process[100]) Leblebici *et al*., found facet-dependent V_{oc} and I_{sc} variations within single grains indicative of facet-dependent defect concentrations.[84] These studies highlight that scanning probe methods are well suited to characterizing nanoscale heterogeneities in perovskite absorber layers and on their surfaces. Such studies allow for determination of connections between morphology and electrical transport properties. However, the requirement for physical interaction between the probe tip and the material itself makes it difficult to characterize buried solid/solid interfaces that are responsible for selective charge extraction. To overcome this limitation, researchers have applied scanning probe methods such as KPFM to device cross sections.[86] Bergmann *et al*. revealed internal electrical potential distributions across the functional layers of a perovskite solar cell by real-space KPFM analysis.[86] It was found that excess holes accumulate in front of the hole selective contact under illumination and thus form an electrical barrier that limits the I_{sc}.[86]

Next, *intra* grain heterogeneity down to the 10×10 nm^2 scale has been reported using high-resolution TEM.[14,89] It appears that grains as they are viewed in the SEM are composed of many sub-crystallites with sizes between ~10-100 nm.[14] Additionally, the presence of twin domains in tetragonal $MAPbI_3$ was discussed by Rothmann *et al*. and is shown in Figure 4f.[89] Twin boundaries impact charge separation, transport, and recombination.[101] The width of the twin domains present in $MAPbI_3$ films range from 100-300 nm and their formation/disappearance is reversible when transitioning through the cubic/tetragonal phase change.[89] This finding might have several implications on device operation because the operation condition of a solar cell spans the

perovskite tetragonal-to-cubic phase transition temperature of ~54 °C.[102] Synthesis of metal halide perovskites typically involves reaction temperatures around 100 °C followed by cooling to room temperature implying a transition from the high symmetry cubic phase to the lower symmetry tetragonal phase. It has been found that crystal twinning is related to this phase transition, possibly as a consequence of releasing internal strain.[89] It would be interesting to do the same study for $MAPbBr_3$, which does not undergo a phase transition at these temperatures and compare the twin densities between the pure I versus Br composition. Furthermore, the appearance of striped domains (blue circles in Figure 4f) with the same orientation before and after heating ("memory effect") may be driven by certain constraints such as strain or high defect densities.[89] This observation is intimately linked to nanoscale heterogeneities and potentially device performance. Furthermore, it is an example where post-growth processing might have a more limited affect than otherwise assumed. If there is such a memory effect, then annealing the films to reduce twins may not be as effective as one might anticipate. Rather, one would need to address the underlying non-ideality that drives twin formation in specific locations, for example by varying and optimizing synthesis.

In addition to explicitly laterally-resolved methods described above, a variety of macroscopic techniques offer powerful potential to unravel chemical compositions and interactions down to the molecular scale. Advanced synchrotron based hard X-ray Photoelectron spectroscopy (HAXPES) has been used to investigate the near surface chemical environment of double, triple and quadruple cation perovskites.[93] Varying the photon energy allowed for chemical composition to be probed at different depths down to ~11 and ~18 nm.[93] Philippe *et al*. found unreacted FAI at the surface of MAFA perovskites, as well as when adding Cs and/or Rb.[93] Rb seems to be mostly located towards the bulk of triple cation RbMAFA compositions while Cs can be found homogeneously distributed

in CsMAFA perovskites.[93] On the other hand, the distribution of Cs and Rb in the quadruple cation perovskite material is rather homogeneous.[93] For molecular-scale compositional and structural information, the combination of synchrotron based X-ray absorption spectroscopy with first-principles density functional theory (DFT) calculations has proven to be very powerful.[90] It is sensitive to the Pb-halide bond lengths, halide chemistry, and octahedral tilting.[90] Finally, solid-state nuclear magnetic resonance (NMR) spectroscopy is a powerful technique to shed light on the microscopic composition of $MAPb(I_{1-x}Br_x)_3$[94] and mixed cation halide perovskites[95,96]. It was recently shown that Rb and K are not incorporated into the perovskite lattice while Cs is incorporated into the lattice with up to 15% in CsFA halide perovskite.[95] This is very interesting because superior device performance and stability were reported for Rb and K containing multi-cation perovskites but leaves us with questions of where are these alkali metals located, in which form are they incorporated, and what is the mechanism that leads to improved device performance? In this respect, it is interesting to compare to chalcogenide thin film solar cell materials such as $Cu(In,Ga)Se_2$, in which it is well known that the alkali metals Na and K play important roles for their optoelectronic properties. In chalcogenides these alkali metals preferentially accumulate along grain boundaries[103] and could induce ion exchange reactions[104]. This research direction is still active and it took many years until some of those findings were broadly accepted. Thus, there is precedent for the expectation that an increasingly active sub-field will evolve within the perovskite community that will focus on mechanistic understanding of the role of alkali metals.

Discussion and Outlook

In summary, hybrid metal halide perovskites are extraordinary semiconductors and represent highly promising building blocks for optoelectronic devices. A variety of studies have revealed heterogeneities with respect to optoelectronic properties, morphology, local recombination, and

transport. However, only a few studies have provided direct causation of local disorder and device performance. Using multiple probes at identical locations at the nanoscale would offer much needed insight into how specific structural and chemical non-idealities and non-uniformities influence optoelectronic properties. However, achieving this aim is not trivial since different methods have different sample requirements. Furthermore, the propensity of hybrid halide perovskites to transform under relatively mild external forces also means that experimental probes can dramatically alter the material. At the same time, a key goal is to characterize how perovskites transform in the presence of electric fields and illumination. Thus, *in situ* tracking of the evolution of perovskites in active devices represents a challenge but has been demonstrated recently employing interdigitated back-contacted substrates.[101]

There are many approaches to synthesizing hybrid halide perovskites. While facile synthesis is an appealing feature of this materials class, it also means that there is wide variability in material quality, absolute composition, and structure. Indeed, most nanoscale studies were performed using "homemade" precursors and according to evolved procedures that have not been rigorously optimized. This raises the question: how generalizable are the findings?

While characterization of isolated perovskite films allows basic material properties to be determined, strong interactions at interfaces can dramatically affect microscopic loss mechanisms and instabilities. In an active device, the perovskite absorber does not exist in isolation and the influence of selective contacts must also be considered. For example, to what degree can insights gained from films on quartz substrates, be applied to films that are located between TiO_2 and spiro-OMeTAD? The presence of these contacting phases leads to electronic and chemical interactions, accumulation of charges, as well as local changes in structure, disorder, and morphology.

Most of the heterogeneities discussed above were investigated in $MAPbI_3$ or $MAPbI_{3-x}Cl_x$ perovskites. More recent multi-cation perovskites (e.g. $KCsFAMAPbI_{3-x}Br_x$) facilitate higher conversion efficiency and wider processing windows and synthesis protocols (as demonstrated for CsMAFA over MAFA[105] or RbCsFA over CsFA[106] compositions). Wider processing windows result in better reproducibility and is the prerequisite for a systematic study of synthesis conditions where uncontrolled variables such as glovebox history are not influencing final film properties. The chemically more complex materials have until now mostly been studied with a focus on device level impact (efficiency and stability) but only very few reports investigated the aspects of evolving/reduced heterogeneities in these multi-components. The intriguing findings of Cs being incorporated into the lattice while Rb and K are not, raise important questions regarding generalizable design rules. Comparison to Na/K-doped chalcogenides gives us a flavor on how distinctly those alkali metals could alter material properties. This leaves plenty of room for exciting new research avenues where composition-function relationships remain to be established. Similarly, 2D-3D perovskite compositions show enhanced device stability but, thus far, reports have mostly focused on device aspects with less attention to dedicated nanoscale characterization. Given the importance of such characterization approaches in advancing understanding of traditional perovskite compounds, such as $MAPbI_3$, it is clear that focus will soon turn to heterogeneous nanoscale structural and optoelectronic properties in these systems. Such studies will be vital for addressing remaining knowledge gaps and for connecting our understanding with that of their 3D counterparts.

Future research will illuminate which nanoscale heterogeneities have to be eliminated to overcome efficiency loss and instabilities or can be exploit for new applications. A better understanding of mechanisms leading to efficiency increase and stability is needed to facilitate

rational optimization of synthesis and composition. In a next level of sophistication, researchers should consider how to use that information to direct synthesis. If, for example, super-grains dominate and define local charge transport, how can their desirable properties be expanded over the full perovskite absorber? Potentially, there is a need for new synthesis routes with targeted growth of certain crystal orientation, controlled nucleation, and strain engineering. In this respect, one avenue here is the development of *in situ* probes to monitor synthesis while the compound is formed. A first step to such a comprehensive strategy to addressing synthesis-function relationships will require connections to be drawn between specific heterogeneities and their influence on macroscopic properties. To conclude, in our opinion there is a strong call for the application of complimentary nondestructive probes that can help to correlate the properties of local disorder with macroscopic function.

ASSOCIATED CONTENT

AUTHOR INFORMATION

Corresponding Author

*E-mail: csutterfella@lbl.gov

Notes

The authors declare no competing financial interest.

Author Contributions

The manuscript was written through contributions of all authors. All authors have given approval to the final version of the manuscript.

Acknowledgements

This manuscript was prepared with support from the Laboratory Directed Research and Development (LDRD) program of Lawrence Berkeley National Laboratory under U.S. Department of Energy contract number DE-AC02-05CH11231 (T.-B.S. and C.M.S.-F.) and by the Solar Photochemistry Program of the U.S. Department of Energy, Office of Science, Office of Basic Energy Sciences, Division of Chemical, Geological and Biosciences under Contract No. DE-AC02-05CH11231 (C.M.S.-F.). I.D.S. acknowledges TUM.Solar in the context of the Bavarian Collaborative Research Project Solar Technologies Go Hybrid (SolTech).

References

(1) Sahli, F.; Werner, J.; Kamino, B. A.; Bräuninger, M.; Monnard, R.; Paviet-Salomon, B.; Barraud, L.; Ding, L.; Leon, J. J. D.; Sacchetto, D.; et al. Fully Textured Monolithic Perovskite/Silicon Tandem Solar Cells with 25.2% Power Conversion Efficiency. *Nat. Mater.* **2018**, 1.

(2) NREL. Research Cell Efficiency Records: Https://Www.Nrel.Gov/Pv/.

(3) Zhang, L.; Yang, X.; Jiang, Q.; Wang, P.; Yin, Z.; Zhang, X.; Tan, H.; Yang, Y. (Michael); Wei, M.; Sutherland, B. R.; et al. Ultra-Bright and Highly Efficient Inorganic Based Perovskite Light-Emitting Diodes. *Nat. Commun.* **2017**, *8*, 15640.

(4) Li, Z.; Moon, J.; Gharajeh, A.; Haroldson, R.; Hawkins, R.; Hu, W.; Zakhidov, A.; Gu, Q. Room-Temperature Continuous-Wave Operation of Organometal Halide Perovskite Lasers. *ArXiv180501092 Phys.* **2018**.

(5) Yin, W.-J.; Shi, T.; Yan, Y. Unique Properties of Halide Perovskites as Possible Origins of the Superior Solar Cell Performance. *Adv. Mater.* **2014**, *26* (27), 4653–4658.

(6) Walsh Aron; Scanlon David O.; Chen Shiyou; Gong X. G.; Wei Su-Huai. Self-Regulation Mechanism for Charged Point Defects in Hybrid Halide Perovskites. *Angew. Chem. Int. Ed.* **2014**, *54* (6), 1791–1794.

(7) Meggiolaro, D.; Motti, S. G.; Mosconi, E.; Barker, A. J.; Ball, J.; Perini, C. A. R.; Deschler, F.; Petrozza, A.; Angelis, F. D. Iodine Chemistry Determines the Defect Tolerance of Lead-Halide Perovskites. *Energy Environ. Sci.* **2018**, *11* (3), 702–713.

(8) Shi, D.; Adinolfi, V.; Comin, R.; Yuan, M.; Alarousu, E.; Buin, A.; Chen, Y.; Hoogland, S.; Rothenberger, A.; Katsiev, K.; et al. Low Trap-State Density and Long Carrier Diffusion in Organolead Trihalide Perovskite Single Crystals. *Science* **2015**, *347* (6221), 519–522.

(9) Stranks, S. D.; Eperon, G. E.; Grancini, G.; Menelaou, C.; Alcocer, M. J. P.; Leijtens, T.; Herz, L. M.; Petrozza, A.; Snaith, H. J. Electron-Hole Diffusion Lengths Exceeding 1 Micrometer in an Organometal Trihalide Perovskite Absorber. *Science* **2013**, *342* (6156), 341–344.

(10) deQuilettes, D. W.; Koch, S.; Burke, S.; Paranji, R. K.; Shropshire, A. J.; Ziffer, M. E.; Ginger, D. S. Photoluminescence Lifetimes Exceeding 8 Ms and Quantum Yields Exceeding 30% in Hybrid Perovskite Thin Films by Ligand Passivation. *ACS Energy Lett.* **2016**, *1* (2), 438–444.

(11) Abdi-Jalebi, M.; Andaji-Garmaroudi, Z.; Cacovich, S.; Stavrakas, C.; Philippe, B.; Richter, J. M.; Alsari, M.; Booker, E. P.; Hutter, E. M.; Pearson, A. J.; et al. Maximizing and Stabilizing Luminescence from Halide Perovskites with Potassium Passivation. *Nature* **2018**, *555* (7697), 497–501.

(12) Hieulle, J.; Stecker, C.; Ohmann, R.; Ono, L. K.; Qi, Y. Scanning Probe Microscopy Applied to Organic–Inorganic Halide Perovskite Materials and Solar Cells. *Small Methods* **2018**, *2* (1), 1700295.

(13) Rothmann, M. U.; Li, W.; Etheridge, J.; Cheng, Y.-B. Microstructural Characterisations of Perovskite Solar Cells – From Grains to Interfaces: Techniques, Features, and Challenges. *Adv. Energy Mater. 7* (23), 1700912.

(14) Jones, T. W.; Osherov, A.; Alsari, M.; Sponseller, M.; Duck, B. C.; Jung, Y.-K.; Settens, C.; Niroui, F.; Brenes, R.; Stan, C. V.; et al. Local Strain Heterogeneity Influences the Optoelectronic Properties of Halide Perovskites. *ArXiv180301192 Cond-Mat* **2018**.

(15) Draguta, S.; Thakur, S.; Morozov, Y. V.; Wang, Y.; Manser, J. S.; Kamat, P. V.; Kuno, M. Spatially Non-Uniform Trap State Densities in Solution-Processed Hybrid Perovskite Thin Films. *J. Phys. Chem. Lett.* **2016**, *7* (4), 715–721.

(16) Bischak, C. G.; Sanehira, E. M.; Precht, J. T.; Luther, J. M.; Ginsberg, N. S. Heterogeneous Charge Carrier Dynamics in Organic–Inorganic Hybrid Materials: Nanoscale Lateral and Depth-Dependent Variation of Recombination Rates in Methylammonium Lead Halide Perovskite Thin Films. *Nano Lett.* **2015**, *15* (7), 4799–4807.

(17) Kutes, Y.; Zhou, Y.; Bosse, J. L.; Steffes, J.; Padture, N. P.; Huey, B. D. Mapping the Photoresponse of CH3NH3PbI3 Hybrid Perovskite Thin Films at the Nanoscale. *Nano Lett.* **2016**, *16* (6), 3434–3441.

(18) Quilettes, D. W. de; Vorpahl, S. M.; Stranks, S. D.; Nagaoka, H.; Eperon, G. E.; Ziffer, M. E.; Snaith, H. J.; Ginger, D. S. Impact of Microstructure on Local Carrier Lifetime in Perovskite Solar Cells. *Science* **2015**, *348* (6235), 683–686.

(19) Tress, W.; Yavari, M.; Domanski, K.; Yadav, P.; Niesen, B.; Baena, J. P. C.; Hagfeldt, A.; Graetzel, M. Interpretation and Evolution of Open-Circuit Voltage, Recombination, Ideality Factor and Subgap Defect States during Reversible Light-Soaking and Irreversible Degradation of

Perovskite Solar Cells. *Energy Environ. Sci.* **2018**, *11* (1), 151–165.

(20) Stranks, S. D.; Snaith, H. J. Metal-Halide Perovskites for Photovoltaic and Light-Emitting Devices. *Nat. Nanotechnol.* **2015**, *10* (5), 391–402.

(21) Paek, S.; Schouwink, P.; Athanasopoulou, E. N.; Cho, K. T.; Grancini, G.; Lee, Y.; Zhang, Y.; Stellacci, F.; Nazeeruddin, M. K.; Gao, P. From Nano- to Micrometer Scale: The Role of Antisolvent Treatment on High Performance Perovskite Solar Cells. *Chem. Mater.* **2017**, *29* (8), 3490–3498.

(22) Alsari, M.; Bikondoa, O.; Bishop, J.; Abdi-Jalebi, M.; Ozer, L. Y.; Hampton, M.; Thompson, P.; Hörantner, M. T.; Mahesh, S.; Greenland, C.; et al. In Situ Simultaneous Photovoltaic and Structural Evolution of Perovskite Solar Cells during Film Formation. *Energy Environ. Sci.* **2018**, *11* (2), 383–393.

(23) Franeker, J. J. van; Hendriks, K. H.; Bruijnaers, B. J.; Verhoeven, M. W. G. M.; Wienk, M. M.; Janssen, R. A. J. Monitoring Thermal Annealing of Perovskite Solar Cells with In Situ Photoluminescence. *Adv. Energy Mater.* **2017**, *7* (7), 1601822.

(24) Li, Y.; Cooper, J. K.; Liu, W.; Sutter-Fella, C. M.; Amani, M.; Beeman, J. W.; Javey, A.; Ager, J. W.; Liu, Y.; Toma, F. M.; et al. Defective TiO2 with High Photoconductive Gain for Efficient and Stable Planar Heterojunction Perovskite Solar Cells. *Nat. Commun.* **2016**, *7*, 12446.

(25) Snaith, H. J.; Abate, A.; Ball, J. M.; Eperon, G. E.; Leijtens, T.; Noel, N. K.; Stranks, S. D.; Wang, J. T.-W.; Wojciechowski, K.; Zhang, W. Anomalous Hysteresis in Perovskite Solar Cells. *J. Phys. Chem. Lett.* **2014**, *5* (9), 1511–1515.

(26) Unger, E. L.; Hoke, E. T.; Bailie, C. D.; Nguyen, W. H.; Bowring, A. R.; Heumüller, T.; Christoforo, M. G.; McGehee, M. D. Hysteresis and Transient Behavior in Current–Voltage Measurements of Hybrid-Perovskite Absorber Solar Cells. *Energy Environ. Sci.* **2014**, *7* (11), 3690–3698.

(27) Kim, H.-S.; Park, N.-G. Parameters Affecting I–V Hysteresis of CH3NH3PbI3 Perovskite Solar Cells: Effects of Perovskite Crystal Size and Mesoporous TiO2 Layer. *J. Phys. Chem. Lett.* **2014**, *5* (17), 2927–2934.

(28) Wu, Y.; Shen, H.; Walter, D.; Jacobs, D.; Duong, T.; Peng, J.; Jiang, L.; Cheng, Y.-B.; Weber, K. On the Origin of Hysteresis in Perovskite Solar Cells. *Adv. Funct. Mater.* **2016**, *26* (37), 6807–6813.

(29) Miller, D. W.; Eperon, G. E.; Roe, E. T.; Warren, C. W.; Snaith, H. J.; Lonergan, M. C. Defect States in Perovskite Solar Cells Associated with Hysteresis and Performance. *Appl. Phys. Lett.* **2016**, *109* (15), 153902.

(30) Yu, H.; Lu, H.; Xie, F.; Zhou, S.; Zhao, N. Native Defect-Induced Hysteresis Behavior in Organolead Iodide Perovskite Solar Cells. *Adv. Funct. Mater.* **2016**, *26* (9), 1411–1419.

(31) Bastiani, M. D.; Dell'Erba, G.; Gandini, M.; D'Innocenzo, V.; Neutzner, S.; Kandada, A. R. S.; Grancini, G.; Binda, M.; Prato, M.; Ball, J. M.; et al. Ion Migration and the Role of Preconditioning Cycles in the Stabilization of the J–V Characteristics of Inverted Hybrid

Perovskite Solar Cells. *Adv. Energy Mater.* **2016**, *6* (2), 1501453.

(32) Li, C.; Tscheuschner, S.; Paulus, F.; Hopkinson, P. E.; Kießling, J.; Köhler, A.; Vaynzof, Y.; Huettner, S. Iodine Migration and Its Effect on Hysteresis in Perovskite Solar Cells. *Adv. Mater.* **2016**, *28* (12), 2446–2454.

(33) Tress, W.; Marinova, N.; Moehl, T.; Zakeeruddin, S. M.; Nazeeruddin, M. K.; Grätzel, M. Understanding the Rate-Dependent J–V Hysteresis, Slow Time Component, and Aging in CH3NH3PbI3 Perovskite Solar Cells: The Role of a Compensated Electric Field. *Energy Environ. Sci.* **2015**, *8* (3), 995–1004.

(34) Kerner, R. A.; Rand, B. P. Linking Chemistry at the TiO2/CH3NH3PbI3 Interface to Current–Voltage Hysteresis. *J. Phys. Chem. Lett.* **2017**, *8* (10), 2298–2303.

(35) Weber, S. A. L.; Hermes, I. M.; Turren-Cruz, S.-H.; Gort, C.; Bergmann, V. W.; Gilson, L.; Hagfeldt, A.; Graetzel, M.; Tress, W.; Berger, R. How the Formation of Interfacial Charge Causes Hysteresis in Perovskite Solar Cells. *Energy Environ. Sci.* **2018**.

(36) Guerrero, A.; Bou, A.; Matt, G.; Almora, O.; Heumüller, T.; Garcia-Belmonte, G.; Bisquert, J.; Hou, Y.; Brabec, C. Switching Off Hysteresis in Perovskite Solar Cells by Fine-Tuning Energy Levels of Extraction Layers. *Adv. Energy Mater.* **2018**, *8* (21), 1703376.

(37) Shao, Y.; Xiao, Z.; Bi, C.; Yuan, Y.; Huang, J. Origin and Elimination of Photocurrent Hysteresis by Fullerene Passivation in $CH_3NH_3PbI_3$ Planar Heterojunction Solar Cells. *Nat. Commun.* **2014**, *5*, 5784.

(38) Shin, S. S.; Yeom, E. J.; Yang, W. S.; Hur, S.; Kim, M. G.; Im, J.; Seo, J.; Noh, J. H.; Seok, S. I. Colloidally Prepared La-Doped BaSnO3 Electrodes for Efficient, Photostable Perovskite Solar Cells. *Science* **2017**, eaam6620.

(39) Wu, Y.; Xie, F.; Chen, H.; Yang, X.; Su, H.; Cai, M.; Zhou, Z.; Noda, T.; Han, L. Thermally Stable MAPbI3 Perovskite Solar Cells with Efficiency of 19.19% and Area over 1 Cm2 Achieved by Additive Engineering. *Adv. Mater.* **2017**, *29* (28), 1701073.

(40) Tang, Z.; Bessho, T.; Awai, F.; Kinoshita, T.; Maitani, M. M.; Jono, R.; Murakami, T. N.; Wang, H.; Kubo, T.; Uchida, S.; et al. Hysteresis-Free Perovskite Solar Cells Made of Potassium-Doped Organometal Halide Perovskite. *Sci. Rep.* **2017**, *7* (1), 12183.

(41) Li, Z.; Tinkham, J.; Schulz, P.; Yang, M.; Kim, D. H.; Berry, J.; Sellinger, A.; Zhu, K. Acid Additives Enhancing the Conductivity of Spiro-OMeTAD Toward High-Efficiency and Hysteresis-Less Planar Perovskite Solar Cells. *Adv. Energy Mater.* **2017**, *7* (4), 1601451.

(42) Son, D.-Y.; Kim, S.-G.; Seo, J.-Y.; Lee, S.-H.; Shin, H.; Lee, D.; Park, N.-G. Universal Approach toward Hysteresis-Free Perovskite Solar Cell via Defect Engineering. *J. Am. Chem. Soc.* **2018**, *140* (4), 1358–1364.

(43) Turren-Cruz, S.-H.; Saliba, M.; Mayer, M. T.; Juárez-Santiesteban, H.; Mathew, X.; Nienhaus, L.; Tress, W.; Erodici, M. P.; Sher, M.-J.; Bawendi, M. G.; et al. Enhanced Charge Carrier Mobility and Lifetime Suppress Hysteresis and Improve Efficiency in Planar Perovskite Solar Cells. *Energy Environ. Sci.* **2018**, *11* (1), 78–86.

(44) Duan, H.-S.; Zhou, H.; Chen, Q.; Sun, P.; Luo, S.; Song, T.-B.; Bob, B.; Yang, Y. The Identification and Characterization of Defect States in Hybrid Organic–Inorganic Perovskite Photovoltaics. *Phys. Chem. Chem. Phys.* **2014**, *17* (1), 112–116.

(45) Sutter-Fella, C. M.; Miller, D. W.; Ngo, Q. P.; Roe, E. T.; Toma, F. M.; Sharp, I. D.; Lonergan, M. C.; Javey, A. Band Tailing and Deep Defect States in CH3NH3Pb(I1–XBrx)3 Perovskites As Revealed by Sub-Bandgap Photocurrent. *ACS Energy Lett.* **2017**, *2* (3), 709–715.

(46) You, J.; Hong, Z.; Yang, Y. (Michael); Chen, Q.; Cai, M.; Song, T.-B.; Chen, C.-C.; Lu, S.; Liu, Y.; Zhou, H.; et al. Low-Temperature Solution-Processed Perovskite Solar Cells with High Efficiency and Flexibility. *ACS Nano* **2014**, *8* (2), 1674–1680.

(47) Adhikari, K. R.; Gurung, S.; Bhattarai, B. K.; Mari, B. Dependence of Perovskite Solar Cells Performance on Temperature and Solar Irradiation. In *2015 3rd International Renewable and Sustainable Energy Conference (IRSEC)*; 2015; pp 1–6.

(48) Samiee, M.; Konduri, S.; Ganapathy, B.; Kottokkaran, R.; Abbas, H. A.; Kitahara, A.; Joshi, P.; Zhang, L.; Noack, M.; Dalal, V. Defect Density and Dielectric Constant in Perovskite Solar Cells. *Appl. Phys. Lett.* **2014**, *105* (15), 153502.

(49) Heo, J. H.; Song, D. H.; Han, H. J.; Kim, S. Y.; Kim, J. H.; Kim, D.; Shin, H. W.; Ahn, T. K.; Wolf, C.; Lee, T.-W.; et al. Planar CH3NH3PbI3 Perovskite Solar Cells with Constant 17.2% Average Power Conversion Efficiency Irrespective of the Scan Rate. *Adv. Mater.* **2015**, *27* (22), 3424–3430.

(50) Zheng, X.; Chen, B.; Dai, J.; Fang, Y.; Bai, Y.; Lin, Y.; Wei, H.; Zeng, X. C.; Huang, J. Defect Passivation in Hybrid Perovskite Solar Cells Using Quaternary Ammonium Halide Anions and Cations. *Nat. Energy* **2017**, *2* (7), 17102.

(51) Green, M. A. General Temperature Dependence of Solar Cell Performance and Implications for Device Modelling. *Prog. Photovolt. Res. Appl.* **2003**, *11* (5), 333–340.

(52) Ono, L. K.; Raga, S. R.; Wang, S.; Kato, Y.; Qi, Y. Temperature-Dependent Hysteresis Effects in Perovskite-Based Solar Cells. *J. Mater. Chem. A* **2015**, *3* (17), 9074–9080.

(53) Heo, S.; Seo, G.; Lee, Y.; Lee, D.; Seol, M.; Lee, J.; Park, J.-B.; Kim, K.; Yun, D.-J.; Kim, Y. S.; et al. Deep Level Trapped Defect Analysis in CH3NH3PbI3 Perovskite Solar Cells by Deep Level Transient Spectroscopy. *Energy Environ. Sci.* **2017**, *10* (5), 1128–1133.

(54) Almora, O.; Aranda, C.; Mas-Marzá, E.; Garcia-Belmonte, G. On Mott-Schottky Analysis Interpretation of Capacitance Measurements in Organometal Perovskite Solar Cells. *Appl. Phys. Lett.* **2016**, *109* (17), 173903.

(55) Saliba, M.; Matsui, T.; Domanski, K.; Seo, J.-Y.; Ummadisingu, A.; Zakeeruddin, S. M.; Correa-Baena, J.-P.; Tress, W. R.; Abate, A.; Hagfeldt, A.; et al. Incorporation of Rubidium Cations into Perovskite Solar Cells Improves Photovoltaic Performance. *Science* **2016**, aah5557.

(56) Tan, H.; Che, F.; Wei, M.; Zhao, Y.; Saidaminov, M. I.; Todorović, P.; Broberg, D.; Walters, G.; Tan, F.; Zhuang, T.; et al. Dipolar Cations Confer Defect Tolerance in Wide-Bandgap Metal Halide Perovskites. *Nat. Commun.* **2018**, *9* (1), 3100.

(57) Yin, W.-J.; Shi, T.; Yan, Y. Unusual Defect Physics in CH3NH3PbI3 Perovskite Solar Cell Absorber. *Appl. Phys. Lett.* **2014**, *104* (6), 063903.

(58) Shockley, W.; Queisser, H. J. Detailed Balance Limit of Efficiency of P-n Junction Solar Cells. *J. Appl. Phys.* **1961**, *32* (3), 510–519.

(59) Sutter-Fella, C. M.; Li, Y.; Amani, M.; Ager, J. W.; Toma, F. M.; Yablonovitch, E.; Sharp, I. D.; Javey, A. High Photoluminescence Quantum Yield in Band Gap Tunable Bromide Containing Mixed Halide Perovskites. *Nano Lett.* **2016**, *16* (1), 800–806.

(60) Deschler, F.; Price, M.; Pathak, S.; Klintberg, L. E.; Jarausch, D.-D.; Higler, R.; Hüttner, S.; Leijtens, T.; Stranks, S. D.; Snaith, H. J.; et al. High Photoluminescence Efficiency and Optically Pumped Lasing in Solution-Processed Mixed Halide Perovskite Semiconductors. *J. Phys. Chem. Lett.* **2014**, *5* (8), 1421–1426.

(61) Xing, G.; Mathews, N.; Lim, S. S.; Yantara, N.; Liu, X.; Sabba, D.; Grätzel, M.; Mhaisalkar, S.; Sum, T. C. Low-Temperature Solution-Processed Wavelength-Tunable Perovskites for Lasing. *Nat. Mater.* **2014**, *13* (5), 476–480.

(62) Stranks, S. D.; Burlakov, V. M.; Leijtens, T.; Ball, J. M.; Goriely, A.; Snaith, H. J. Recombination Kinetics in Organic-Inorganic Perovskites: Excitons, Free Charge, and Subgap States. *Phys. Rev. Appl.* **2014**, *2* (3), 034007.

(63) Stranks, S. D. Nonradiative Losses in Metal Halide Perovskites. *ACS Energy Lett.* **2017**, *2* (7), 1515–1525.

(64) Brenes, R.; Guo, D.; Osherov, A.; Noel, N. K.; Eames, C.; Hutter, E. M.; Pathak, S. K.; Niroui, F.; Friend, R. H.; Islam, M. S.; et al. Metal Halide Perovskite Polycrystalline Films Exhibiting Properties of Single Crystals. *Joule* **2017**, *1* (1), 155–167.

(65) Sutter-Fella, C. M.; Ngo, Q. P.; Cefarin, N.; Gardner, K. L.; Tamura, N.; Stan, C. V.; Drisdell, W. S.; Javey, A.; Toma, F. M.; Sharp, I. D. Cation-Dependent Light-Induced Halide Demixing in Hybrid Organic–Inorganic Perovskites. *Nano Lett.* **2018**, *18* (6), 3473–3480.

(66) Rajagopal, A.; Stoddard, R. J.; Jo, S. B.; Hillhouse, H. W.; Jen, A. K.-Y. Overcoming the Photovoltage Plateau in Large Bandgap Perovskite Photovoltaics. *Nano Lett.* **2018**, *18* (6), 3985–3993.

(67) Jacobsson, T. J.; Correa-Baena, J.-P.; Pazoki, M.; Saliba, M.; Schenk, K.; Grätzel, M.; Hagfeldt, A. Exploration of the Compositional Space for Mixed Lead Halogen Perovskites for High Efficiency Solar Cells. *Energy Environ. Sci.* **2016**, *9* (5), 1706–1724.

(68) Zhou, Y.; Jia, Y.-H.; Fang, H.-H.; Loi, M. A.; Xie, F.-Y.; Gong, L.; Qin, M.-C.; Lu, X.-H.; Wong, C.-P.; Zhao, N. Composition-Tuned Wide Bandgap Perovskites: From Grain Engineering to Stability and Performance Improvement. *Adv. Funct. Mater. 0* (0), 1803130.

(69) Motti, S. G.; Gandini, M.; Barker, A. J.; Ball, J. M.; Srimath Kandada, A. R.; Petrozza, A. Photoinduced Emissive Trap States in Lead Halide Perovskite Semiconductors. *ACS Energy Lett.* **2016**, *1* (4), 726–730.

(70) Richter, J. M.; Abdi-Jalebi, M.; Sadhanala, A.; Tabachnyk, M.; Rivett, J. P. H.; Pazos-Outón, L. M.; Gödel, K. C.; Price, M.; Deschler, F.; Friend, R. H. Enhancing Photoluminescence Yields in Lead Halide Perovskites by Photon Recycling and Light Out-Coupling. *Nat. Commun.* **2016**, *7*, 13941.

(71) Ross, R. T. Some Thermodynamics of Photochemical Systems. *J. Chem. Phys.* **1967**, *46* (12), 4590–4593.

(72) Smestad, G.; Ries, H. Luminescence and Current-Voltage Characteristics of Solar Cells and Optoelectronic Devices. *Sol. Energy Mater. Sol. Cells* **1992**, *25* (1), 51–71.

(73) Rau, U. Reciprocity Relation between Photovoltaic Quantum Efficiency and Electroluminescent Emission of Solar Cells. *Phys. Rev. B* **2007**, *76* (8), 085303.

(74) Green, M. A. Radiative Efficiency of State-of-the-Art Photovoltaic Cells. *Prog. Photovolt. Res. Appl.* **2012**, *20* (4), 472–476.

(75) Hoke, E. T.; Slotcavage, D. J.; Dohner, E. R.; Bowring, A. R.; Karunadasa, H. I.; McGehee, M. D. Reversible Photo-Induced Trap Formation in Mixed-Halide Hybrid Perovskites for Photovoltaics. *Chem. Sci.* **2014**, *6* (1), 613–617.

(76) McMeekin, D. P.; Sadoughi, G.; Rehman, W.; Eperon, G. E.; Saliba, M.; Hörantner, M. T.; Haghighirad, A.; Sakai, N.; Korte, L.; Rech, B.; et al. A Mixed-Cation Lead Mixed-Halide Perovskite Absorber for Tandem Solar Cells. *Science* **2016**, *351* (6269), 151–155.

(77) Chen, A. Z.; Shiu, M.; Ma, J. H.; Alpert, M. R.; Zhang, D.; Foley, B. J.; Smilgies, D.-M.; Lee, S.-H.; Choi, J. J. Origin of Vertical Orientation in Two-Dimensional Metal Halide Perovskites and Its Effect on Photovoltaic Performance. *Nat. Commun.* **2018**, *9* (1), 1336.

(78) Cho, Y.; Soufiani, A. M.; Yun, J. S.; Kim, J.; Lee, D. S.; Seidel, J.; Deng, X.; Green, M. A.; Huang, S.; Ho-Baillie, A. W. Y. Mixed 3D–2D Passivation Treatment for Mixed-Cation Lead Mixed-Halide Perovskite Solar Cells for Higher Efficiency and Better Stability. *Adv. Energy Mater.* **2018**, *8* (20), 1703392.

(79) Herz, L. M. Charge-Carrier Mobilities in Metal Halide Perovskites: Fundamental Mechanisms and Limits. *ACS Energy Lett.* **2017**, *2* (7), 1539–1548.

(80) Levine, I.; Gupta, S.; Bera, A.; Ceratti, D.; Hodes, G.; Cahen, D.; Guo, D.; Savenije, T. J.; Ávila, J.; Bolink, H. J.; et al. Can We Use Time-Resolved Measurements to Get Steady-State Transport Data for Halide Perovskites? *J. Appl. Phys.* **2018**, *124* (10), 103103.

(81) Quilettes, D. W. de; Vorpahl, S. M.; Stranks, S. D.; Nagaoka, H.; Eperon, G. E.; Ziffer, M. E.; Snaith, H. J.; Ginger, D. S. Impact of Microstructure on Local Carrier Lifetime in Perovskite Solar Cells. *Science* **2015**, *348* (6235), 683–686.

(82) Vrućinić, M.; Matthiesen, C.; Sadhanala, A.; Divitini, G.; Cacovich, S.; Dutton, S. E.; Ducati, C.; Atatüre, M.; Snaith, H.; Friend, R. H.; et al. Local Versus Long-Range Diffusion Effects of Photoexcited States on Radiative Recombination in Organic–Inorganic Lead Halide Perovskites. *Adv. Sci. 2* (9), 1500136.

(83) Bischak, C. G.; Hetherington, C. L.; Wu, H.; Aloni, S.; Ogletree, D. F.; Limmer, D. T.; Ginsberg, N. S. Origin of Reversible Photoinduced Phase Separation in Hybrid Perovskites. *Nano Lett.* **2017**, *17* (2), 1028–1033.

(84) Leblebici, S. Y.; Leppert, L.; Li, Y.; Reyes-Lillo, S. E.; Wickenburg, S.; Wong, E.; Lee, J.; Melli, M.; Ziegler, D.; Angell, D. K.; et al. Facet-Dependent Photovoltaic Efficiency Variations in Single Grains of Hybrid Halide Perovskite. *Nat. Energy* **2016**, *1* (8), 16093.

(85) Edri, E.; Kirmayer, S.; Mukhopadhyay, S.; Gartsman, K.; Hodes, G.; Cahen, D. Elucidating the Charge Carrier Separation and Working Mechanism of $CH_3NH_3PbI_{3-x}Cl_x$ Perovskite Solar Cells. *Nat. Commun.* **2014**, *5*, 3461.

(86) Bergmann, V. W.; Weber, S. A. L.; Ramos, F. J.; Nazeeruddin, M. K.; Grätzel, M.; Li, D.; Domanski, A. L.; Lieberwirth, I.; Ahmad, S.; Berger, R. Real-Space Observation of Unbalanced Charge Distribution inside a Perovskite-Sensitized Solar Cell. *Nat. Commun.* **2014**, *5*, 5001.

(87) Dymshits, A.; Henning, A.; Segev, G.; Rosenwaks, Y.; Etgar, L. The Electronic Structure of Metal Oxide/Organo Metal Halide Perovskite Junctions in Perovskite Based Solar Cells. *Sci. Rep.* **2015**, *5*, 8704.

(88) Garrett, J. L.; Tennyson, E. M.; Hu, M.; Huang, J.; Munday, J. N.; Leite, M. S. Real-Time Nanoscale Open-Circuit Voltage Dynamics of Perovskite Solar Cells. *Nano Lett.* **2017**, *17* (4), 2554–2560.

(89) Rothmann, M. U.; Li, W.; Zhu, Y.; Bach, U.; Spiccia, L.; Etheridge, J.; Cheng, Y.-B. Direct Observation of Intrinsic Twin Domains in Tetragonal $CH_3NH_3PbI_3$. *Nat. Commun.* **2017**, *8*, 14547.

(90) Drisdell, W. S.; Leppert, L.; Sutter-Fella, C. M.; Liang, Y.; Li, Y.; Ngo, Q. P.; Wan, L. F.; Gul, S.; Kroll, T.; Sokaras, D.; et al. Determining Atomic-Scale Structure and Composition of Organo-Lead Halide Perovskites by Combining High-Resolution X-Ray Absorption Spectroscopy and First-Principles Calculations. *ACS Energy Lett.* **2017**, *2* (5), 1183–1189.

(91) Vorwerk, C.; Hartmann, C.; Cocchi, C.; Sadoughi, G.; Habisreutinger, S. N.; Félix, R.; Wilks, R. G.; Snaith, H. J.; Bär, M.; Draxl, C. Exciton-Dominated Core-Level Absorption Spectra of Hybrid Organic–Inorganic Lead Halide Perovskites. *J. Phys. Chem. Lett.* **2018**, *9* (8), 1852–1858.

(92) Abdelmageed, G.; Jewell, L.; Hellier, K.; Seymour, L.; Luo, B.; Bridges, F.; Zhang, J. Z.; Carter, S. Mechanisms for Light Induced Degradation in MAPbI3 Perovskite Thin Films and Solar Cells. *Appl. Phys. Lett.* **2016**, *109* (23), 233905.

(93) Philippe, B.; Saliba, M.; Correa-Baena, J.-P.; Cappel, U. B.; Turren-Cruz, S.-H.; Grätzel, M.; Hagfeldt, A.; Rensmo, H. Chemical Distribution of Multiple Cation (Rb+, Cs+, MA+, and FA+) Perovskite Materials by Photoelectron Spectroscopy. *Chem. Mater.* **2017**, *29* (8), 3589–3596.

(94) Rosales, B. A.; Hanrahan, M. P.; Boote, B. W.; Rossini, A. J.; Smith, E. A.; Vela, J. Lead Halide Perovskites: Challenges and Opportunities in Advanced Synthesis and Spectroscopy. *ACS Energy Lett.* **2017**, *2* (4), 906–914.

(95) Kubicki, D. J.; Prochowicz, D.; Hofstetter, A.; Zakeeruddin, S. M.; Grätzel, M.; Emsley, L. Phase Segregation in Cs-, Rb- and K-Doped Mixed-Cation (MA)x(FA)1–XPbI3 Hybrid Perovskites from Solid-State NMR. *J. Am. Chem. Soc.* **2017**, *139* (40), 14173–14180.

(96) Kubicki, D. J.; Prochowicz, D.; Hofstetter, A.; Péchy, P.; Zakeeruddin, S. M.; Grätzel, M.; Emsley, L. Cation Dynamics in Mixed-Cation (MA)x(FA)1–XPbI3 Hybrid Perovskites from Solid-State NMR. *J. Am. Chem. Soc.* **2017**, *139* (29), 10055–10061.

(97) Braly, I. L.; deQuilettes, D. W.; Pazos-Outón, L. M.; Burke, S.; Ziffer, M. E.; Ginger, D. S.; Hillhouse, H. W. Hybrid Perovskite Films Approaching the Radiative Limit with over 90% Photoluminescence Quantum Efficiency. *Nat. Photonics* **2018**, *12* (6), 355–361.

(98) Xiao, C.; Li, Z.; Guthrey, H.; Moseley, J.; Yang, Y.; Wozny, S.; Moutinho, H.; To, B.; Berry, J. J.; Gorman, B.; et al. Mechanisms of Electron-Beam-Induced Damage in Perovskite Thin Films Revealed by Cathodoluminescence Spectroscopy. *J. Phys. Chem. C* **2015**, *119* (48), 26904–26911.

(99) Hentz, O.; Zhao, Z.; Gradečak, S. Direct Correlation between Local Stoichiometry and Optoelectronic Properties in CH3NH3PbI3films. In *2016 IEEE 43rd Photovoltaic Specialists Conference (PVSC)*; 2016; pp 3661–3663.

(100) Li, Y.; Cooper, J. K.; Buonsanti, R.; Giannini, C.; Liu, Y.; Toma, F. M.; Sharp, I. D. Fabrication of Planar Heterojunction Perovskite Solar Cells by Controlled Low-Pressure Vapor Annealing. *J. Phys. Chem. Lett.* **2015**, *6* (3), 493–499.

(101) Brown, E.; Sheng, C.; Shimamura, K.; Shimojo, F.; Nakano, A. Enhanced Charge Recombination Due to Surfaces and Twin Defects in GaAs Nanostructures. *J. Appl. Phys.* **2015**, *117* (5), 054307.

(102) Poglitsch, A.; Weber, D. Dynamic Disorder in Methylammoniumtrihalogenoplumbates (II) Observed by Millimeter-wave Spectroscopy. *J. Chem. Phys.* **1987**, *87* (11), 6373–6378.

(103) Reinhard, P.; Bissig, B.; Pianezzi, F.; Avancini, E.; Hagendorfer, H.; Keller, D.; Fuchs, P.; Döbeli, M.; Vigo, C.; Crivelli, P.; et al. Features of KF and NaF Postdeposition Treatments of Cu(In,Ga)Se2 Absorbers for High Efficiency Thin Film Solar Cells. *Chem. Mater.* **2015**, *27* (16), 5755–5764.

(104) Chirilă, A.; Reinhard, P.; Pianezzi, F.; Bloesch, P.; Uhl, A. R.; Fella, C.; Kranz, L.; Keller, D.; Gretener, C.; Hagendorfer, H.; et al. Potassium-Induced Surface Modification of $Cu(In,Ga)Se_2$ Thin Films for High-Efficiency Solar Cells. *Nat. Mater.* **2013**, *12* (12), 1107–1111.

(105) Saliba, M.; Matsui, T.; Seo, J.-Y.; Domanski, K.; Correa-Baena, J.-P.; Nazeeruddin, M. K.; Zakeeruddin, S. M.; Tress, W.; Abate, A.; Hagfeldt, A.; et al. Cesium-Containing Triple Cation Perovskite Solar Cells: Improved Stability, Reproducibility and High Efficiency. *Energy Environ. Sci.* **2016**, *9* (6), 1989–1997.

(106) Turren-Cruz, S.-H.; Hagfeldt, A.; Saliba, M. Methylammonium-Free, High-Performance and Stable Perovskite Solar Cells on a Planar Architecture. *Science* **2018**, DOI: 10.1126/science.aat3583.